Fluoride Inhibition of Bovine Spleen Purple Acid Phosphatase: Characterization of a Ternary Enzyme−Phosphate−Fluoride Complex as a Model for the Active Enzyme−Substrate−Hydroxide Complex

Martijn W. H. Pinkse, Maarten Merkx, and Bruce A. Averill*

E.C. Slater Institute, Biocentrum Amsterdam, University of Amsterdam, Plantage Muidergracht 12, 1018 TV, Amsterdam, The Netherlands

Received February 24, 1999; Revised Manuscript Received June 7, 1999

ABSTRACT: Purple acid phosphatases (PAPs) employ a dinuclear $Fe^{3+}Fe^{2+}$ or $Fe^{3+}Zn^{2+}$ center to catalyze the hydrolysis of phosphate monoesters. The interaction of fluoride with bovine spleen purple acid phosphatase (BSPAP) has been studied using a combination of steady-state kinetics and spectroscopic methods. For FeZn−BSPAP, the nature of the inhibition changes from noncompetitive at pH 6.5 ($K_{i(comp)} \approx K_{i(uncomp)} \approx 2$ mM) to uncompetitive at pH 5.0 ($K_{i(uncomp)} = 0.2$ mM). The inhibition constant for AlZn−BSPAP at pH 5.0 ($K_i = 3$ μM) is ∼50−70-fold lower than that observed for both FeZn−BSAP and GaZn−BSPAP, suggesting that fluoride binds to the trivalent metal. Fluoride binding to the enzyme−substrate complex was found to be remarkably slow; hence, the kinetics of fluoride binding were studied in some detail for FeZn−, AlZn−, and FeFe−BSPAP at pH 5.0 and for FeZn−BSPAP at pH 6.5. Since the enzyme kinetics studies indicated the formation of a ternary enzyme−substrate-fluoride complex, the binding of fluoride to FeZn−BSPAP was studied using optical and EPR spectroscopies, both in the presence and absence of phosphate. The characteristic optical and EPR spectra of FeZn−BSPAP·F and FeZn−BSPAP·PO_4·F are similar at pH 5.0 and pH 6.5, indicating the formation of similar fluoride complexes at both pHs. A structural model for the ternary enzyme−(substrate/phosphate)-fluoride complexes is proposed that can explain the results from both the spectroscopic and the enzyme kinetics experiments. In this model, fluoride binds to the trivalent metal replacing the water/hydroxide ligand that is essential for the hydrolysis reaction to take place, while phosphate or the phosphate ester coordinates to the divalent metal ion.

Purple acid phosphatases (PAPs)[1] belong to the growing group of metalloenzymes that employ a di- or trinuclear metal center to catalyze hydrolysis reactions (*1*, *2*). All mammalian PAPs contain a diiron center, which is catalytically active in the mixed-valent Fe(III)−Fe(II) oxidation state (*3*). Two of those have been the subject of extensive spectroscopic and enzyme kinetics studies, uteroferrin (isolated from the uteral fluids of pregnant pigs; Uf) and bovine spleen purple acid phosphatase (BSPAP). The plant PAP isolated from red kidney beans (KBPAP) is the only PAP for which an X-ray structure has been determined (*4*, *5*). This PAP contains an Fe(III)Zn(II) metal center, but shows kinetics and spectroscopic properties similar to those of the mammalian enzymes. All amino acids found to coordinate the metals in KBPAP are strictly conserved among all PAP sequences, even those from microorganisms such as *Aspergillus ficum* (*3*, *6*). Moreover, a sequence motif that incorporates most of these amino acids is found in a much larger group of phosphohydrolases, among which are exonucleases, 5′-nucleotidases, diadenosinetetraphosphatases, and Ser/Thr specific protein phosphatases (*5*, *7*, *8*). X-ray structure determinations of two Ser/Thr specific protein phosphatases, PP1 and PP2B (calcineurin), have revealed a dinuclear metal center resembling that of the PAPs, except for the tyrosinate ligand to the Fe^{3+} that gives the PAPs their characteristic purple color. The PAPs have a number of properties that permit the molecular details by which these dinuclear metal centers participate in the hydrolysis of phosphate esters to be studied: (1) they have favorable spectroscopic properties (intense charge-transfer band, characteristic EPR signals in the active Fe(III)-Fe(II) and Fe(III)Zn(II) oxidation states, Mössbauer active metal ions) that provide probes to follow processes taking place in the coordination environment of the metal center; (2) unlike the PPs, the PAPs are relatively stable enzymes whose activity is not regulated via complicated activation mechanisms; (3) each of the two metals can be specifically

* To whom correspondence should be addressed. Telephone: 31-20-5255045. Fax: 31-20-5255124. E-mail: BAA@chem.uva.nl.

[1] Abbreviations: AlZn−BSPAP, BSPAP with aluminum at the ferric site and zinc at the ferrous site; BSPAP, bovine spleen purple acid phosphatase; EPR, electron paramagnetic resonance; EXAFS, extended X-ray absorption fine structure; FeFe−BSPAP, BSPAP with iron at the ferric and ferrous sites; FeZn−BSPAP, BSPAP with iron at the ferric site and zinc at the ferrous site; FeZn−BSPAP·F, FeZn−BSPAP complexed with fluoride; FeZn−BSPAP·PO_4, FeZn−BSPAP complexed with phosphate; FeZn−BSPAP·PO_4·F, FeZn−BSPAP complexed with phosphate and fluoride; FeZn−Uf, uteroferrin with iron at the ferric site and zinc at the ferrous site; GaZn−BSPAP, BSPAP with gallium at the ferric site and zinc at the ferrous site; KBPAP, purple acid phosphatase of red kidney beans; MES, 2-[N-morpholino]-ethanesulfonic acid; PAP, purple acid phosphatase; *p*-NPP, disodium salt of *p*-nitrophenyl phosphate; PP, protein phosphatase; PP1, protein phosphatase 1; PP2B, protein phosphatase 2B; Uf, uteroferrin.

10.1021/bi990446w CCC: $18.00
Published on Web 07/20/1999

substituted by other metal ions. This latter property has been used recently to study the specific chemical requirements for the trivalent metal ion (*9*). Moreover, Fe(III)Zn(II)−PAP may be used to study the effect of inhibitors such as phosphate on each of the two metal ions separately via, e.g., EXAFS and EPR spectroscopic studies (*10*−*13*).

BSPAP has been shown to catalyze the hydrolysis of the chiral substrate S_p-2′,3′-methoxymethylidene-ATP-$\gamma S\gamma^{18}O\gamma^{17}O$ with overall inversion of the configuration of the phosphorus, which supports a mechanism in which the phosphate ester is directly attacked by water, without the existence of a phosphoenzyme intermediate (*14*). The absence of burst kinetics has been explained by a model in which the attack of an activated water or hydroxide on the phosphate ester is the rate-limiting step in catalysis, rather than, e.g., release of phosphate from the enzyme (*13*). The coordination of phosphate and other oxoanions that inhibit PAP has been studied in some detail using a variety of spectroscopic techniques, since these inhibitors were assumed to mimic the binding of the phosphate monoester substrate. In the preceding paper, we reported that the coordination mode of phosphate is pH dependent. At pH 5, phosphate binds to both the Fe^{3+} and the divalent metal ion via a bridging coordination mode. At pH 6.5, however, we proposed that hydroxide replaces the phosphate at the Fe^{3+} site, and phosphate coordinates to only the divalent metal ion. It seems likely that the structure of the phosphate complex at pH 6.5 approximates that of the active state of the enzyme−substrate complex, since rapid-mixing rapid-freezing experiments showed very similar EPR spectral properties for the phosphate and substrate complexes, both at pH 5 and pH 6.5 (*13*).

Fluoride has long been known to inhibit PAP catalysis (*15*−*25*), and spectroscopic studies indicate that fluoride binds directly to the metal center (*23*, *24*, *26*). Fluoride stimulates bone cell proliferation and activity and has, therefore, been used to treat patients with osteoporosis. Several pieces of evidence indicate that this effect of fluoride may be due to the inhibition of bone PAP (*27*). An Fe^{3+}-bound hydroxide is assumed to play a critical role in catalysis, either directly as the nucleophile that attacks the substrate (*5*, *28*) or as a general base that deprotonates a water in the second coordination sphere of the trivalent metal ion (*9*). Since fluoride has chemical properties similar to hydroxide, studying fluoride inhibition may reveal the coordination chemistry of the other substrate of the hydrolysis reaction, i.e., water/hydroxide. For example, a study of fluoride inhibition of the dinuclear aminopeptidase from *Aeromonas proteolytica* recently resulted in the identification of a Zn(II)-bound water/hydroxide with a pK_a value of 7.0 in the enzyme−substrate complex (*29*).

We studied the nature of fluoride binding to Fe(III)Zn(II)−BSPAP at various pHs from 6.5 to 5.0 using steady-state kinetics methods. The availability of metal-substitituted forms of BSPAP with different trivalent metal ions enabled us to examine the effect of the nature of the trivalent metal on the affinity for fluoride and provided strong evidence for coordination of fluoride to the trivalent metal ion. The finding that fluoride binding to AlZn−BSPAP is surprisingly slow prompted us to study the kinetics of fluoride binding in more detail. Optical and EPR spectroscopy were used to study the binding of fluoride, both in the presence and in the absence of phosphate. A model is presented for the structure of the ternary enzyme−substrate/phosphate/fluoride complex(es) that explains the results from both the enzyme kinetics and the spectroscopic experiments.

EXPERIMENTAL PROCEDURES

General. Bovine spleen purple acid phosphatase was isolated as previously described (*30*). Preparations had $A_{280\ nm}/A_{536\ nm}$ ratios of 14−15. FeZn−BSPAP, GaZn−BSPAP, and AlZn−BSPAP were prepared as described previously (*9*, *30*). Protein concentrations of native BSPAP and FeZn−BSPAP were determined by measuring the absorption of the tyrosinate-to-Fe^{3+} charge-transfer band at ∼530 nm (ϵ = 4080 $M^{-1}\cdot cm^{-1}$). Optical spectra were measured on a Cary 50 spectrophotometer (Varian).

Steady-State Enzyme Kinetics. Enzyme assays using *p*-NPP as a substrate (pH 5.5−6.5) were performed as previously described (*30*). At pH 5.0, phosphatase activity was assayed by monitoring the formation of phenol from the hydrolysis of phenyl phosphate at 278 nm (ϵ = 870 $M^{-1}\cdot cm^{-1}$). FeFe−BSPAP was assayed in 100 mM Na−MES, 185 mM KCl, 15 mM Na−ascorbate, 0.2 mM $Fe(NH_4)_2(SO_4)_2$, pH 6.5. At pH 6.0−6.5, the activity of FeZn−BSPAP was measured in 100 mM Na−MES and 200 mM KCl. Assays at pH 5.5−5.0 were performed in 100 mM NaOAc and 200 mM KCl. All assays were done at 22 °C. Fluoride inhibition was studied by measuring phosphatase activities for nine substrate concentrations at 4−5 different fluoride concentrations. Values of $K_{i(comp)}$ and $K_{i(uncomp)}$ were obtained by fitting the entire data set to the Michaelis−Menten equation for mixed-competitive inhibition using the program MacCurveFit 1.4 (Kevin Raner Software). For AlZn−BSPAP, the rate of phosphate hydrolysis was determined after this rate had become constant (app 30−60 s after the start of the reaction).

Kinetics of Slow Fluoride Binding. The kinetics of fluoride binding were studied by rapidly mixing enzyme with substrate and fluoride using an RX1000 hand-stopped flow device (Applied Photophysics) attached to a Cary 50 spectrophotometer (Varian). One syringe contained enzyme, while the other syringe contained substrate and fluoride. Reactions at pH 6.5 were done in 100 mM Na−MES, 200 mM KCl, pH 6.5 with 50 mM *p*-NPP as the substrate. Reactions at pH 5.0 were done in100 mM NaOAc, 200 mM KCl, pH 5.0 with 25 mM phenyl phosphate as the substrate. Values of k_{obs} were obtained by fitting the progress curves to eq 2 using the nonlinear fit procedure of the program IGOR 3.1 (WaveMetrics).

EPR Spectroscopy. X-band EPR spectra (9.4 GHz) were obtained on a Bruker ECS106 EPR spectrometer, equipped with an Oxford Instruments ESR900 helium-flow cryostat with an ITC4 temperature controller. The magnetic field was calibrated with an AEG Magnetic Field Meter. The frequency was measured with an HP 5350B Microwave Frequency Counter.

Fluoride titrations of FeZn−BSPAP were performed by repeated addition of small aliquots of concentrated KF stock solutions of the appropriate pH to a single sample of FeZn−BSPAP or FeZn−BSPAP·PO_4 in 100 mM buffer (NaOAc/pH 5 or Na-MES/pH 6.5) and 200 mM KCl. Spectral amplitudes and anion concentrations were corrected for dilution. K_d values were determined as previously described (*9*).

Time-Resolved Spectroscopy of FeZn−BSPAP·PO_4·F−Complex Formation. The formation of FeZn−BSPAP·PO_4·F was followed by both optical and EPR spectroscopy. FeZn−BSPAP (∼20 μM) in 100 mM NaOAc, 200 mM KCl, pH 5.0 was rapidly mixed with 1 mM KF and 25 mM KH_2PO_4 (final concentrations) using an RX1000 hand-stopped flow device attached to an HP8452A diode array spectrophotometer, and spectra were collected every second. As a background spectrum, the spectrum of FeZn−BSPAP·PO_4·F complex at equilibrium was used. For EPR, 15 μM FeZn−BSPAP in 100 mM NaOAc, 200 mM KCl, pH 5.0 was rapidly mixed with 1 mM KF and 25 mM KH_2PO_4 (final concentrations) using a home-built rapid-mixing freeze-quench apparatus (*31*) and injected into EPR tubes. At several times after mixing, the samples in the EPR tubes were rapidly frozen in a bath of liquid isopentane (∼140 K).

RESULTS

In the preceding paper in this issue, it was shown that studying the binding of the inhibitor phosphate can provide important insights into the interaction of the substrate *p*-NPP with the dimetal active site. In this report, a similar approach was followed to learn more about the other substrate of the hydrolysis reaction, the nucleophilic hydroxide or water, by studying the interaction of BSPAP with fluoride, an inhibitor that is a structural analogue of hydroxide. The inhibition of Fe(III)Zn(II)−BSPAP by fluoride was studied at several pHs from 6.5 to 5.0. *p*-NPP was used as a substrate at pH 6.5−5.5, while phenyl phosphate was used at pH 5.0. At pH 5.0, the K_M for *p*-NPP becomes too low to allow the reliable determination of K_M values, especially in the presence of fluoride, which lowers the apparent K_M. The K_M for phenyl phosphate is somewhat higher, and its hydrolysis can be studied continuously at 278 nm. Figure 1 shows Lineweaver−Burke plots in the presence of various fluoride concentrations at pH 5.0 and pH 6.5. At pH 5.0, the Lineweaver−Burke plot shows parallel lines, which is indicative of uncompetitive inhibition. However, parallel lines in the double-reciprocal plots can also result from partial uncompetitive inhibition. Plots of $1/K_{M(apparent)}$ and $1/V_{max(apparent)}$ are linear for FeZn−BSPAP at pH 5.0, showing that fluoride is a pure uncompetitive inhibitor (Figure S2 of the Supporting Information) (*32*). At pH 6.5, the lines of the Lineweaver−Burke plot intersect at a single point close to the $1/S$ axis, which is characteristic of noncompetitive inhibition, so $K_{i(comp)} \approx K_{i(uncomp)}$. Scheme 1 shows a kinetic scheme that includes both competitive and uncompetitive inhibition, while eq 1 is the Michaelis−Menten equation for this kinetic scheme.

$$v = V_{max}[S]/(K_s(1 + [I]/K_{i(comp)}) + [S](1 + [I]/K_{i(uncomp)})) \quad (1)$$

Fluoride inhibition was also studied at pH 6.0 and 5.5 (Figure S1 of the Supporting Information). The K_i for the uncompetitive site decreases upon lowering the pH, while the K_i for the competitive site seems to be unaffected, resulting in essentially uncompetitive inhibition at pH 5.0 (Table 1). The pH dependence of $K_{i(uncomp)}$ parallels the pK_a of the Fe^{3+}-coordinated water in the enzyme−substrate complex identified in the preceding paper, suggesting that the uncompetitive

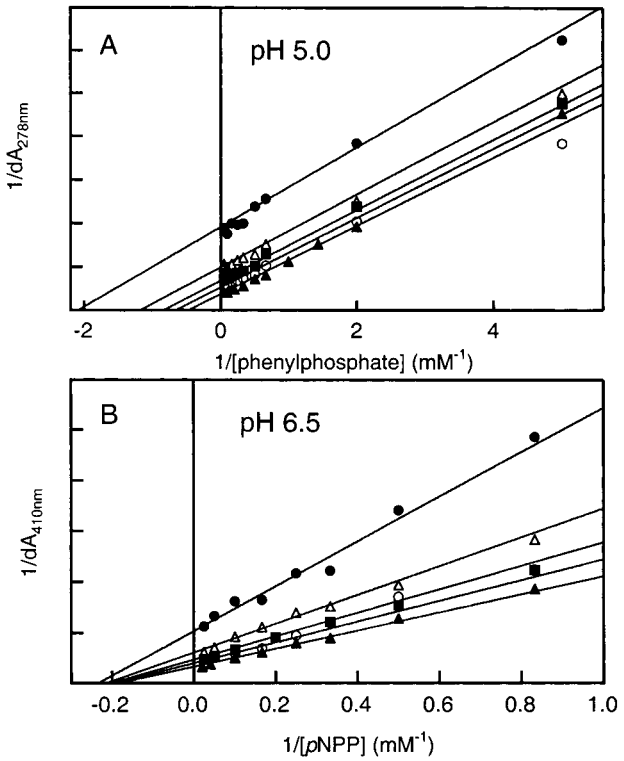

FIGURE 1: Lineweaver−Burke plots of inhibition of FeZn−BSPAP by fluoride at (A) pH 5.0 and (B) pH 6.5. The lines result from a fit of the entire data set to the Michaelis−Menten equation for mixed-competitive inhibition (see Table 1 for K_i values obtained from these fits). Conditions: (A) phenyl phosphate in 100 mM NaOAc, 200 mM KCl pH 5.0, 22 °C, with 0, 0.10, 0.20, 0.40, and 1.0 mM fluoride; (B) *p*-NPP in 100 mM Na−MES, 200 mM KCl, pH 6.5, 22 °C, with 0, 0.50, 1.0, 2.0, and 5.0 mM fluoride.

Scheme 1

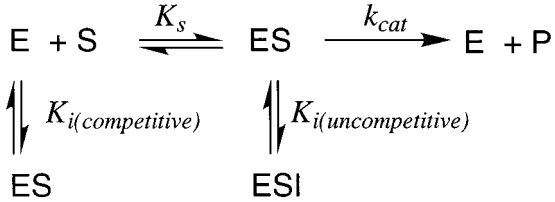

binding site of fluoride is at the trivalent metal. If the uncompetitive binding site of fluoride is indeed at the trivalent metal, the chemical nature of the trivalent metal is expected to affect $K_{i(uncomp)}$. Fluoride inhibition was, therefore, also studied for AlZn−BSPAP and GaZn−BSPAP at pH 5.0 (Figure S1 and S2). Both GaZn−BSPAP and AlZn−BSPAP are uncompetitively inhibited by fluoride at pH 5.0 (Table 1). The inhibition constant for AlZn−BSPAP is ∼50−70-fold lower than the inhibition constants for both FeZn−BSAP and GaZn−BSPAP, indicating that the uncompetitive binding site of fluoride is indeed at the trivalent metal ion.

The steady-state kinetic results indicated that in the presence of substrate fluoride binds at the trivalent metal ion. This interaction can be directly probed by studying the effect of fluoride on the optical and EPR spectra of the enzyme. For FeZn−BSPAP, both techniques are expected to detect changes in the immediate coordination environment of the Fe^{3+} and to be much less sensitive to fluoride binding at the divalent metal site. The binding of fluoride to FeZn−BSPAP was studied both in the absence and presence of phosphate, which was assumed to mimic the binding of

Table 1: Inhibition Constants for Inhibition of Various Metal-Substituted BSPAP Forms by Fluoride[a]

enzyme	pH	substrate	K_i competitive (mM)	K_i uncompetitive (mM)
FeZn[b]	5.0	phenylphosphate		0.20 (0.03)
AlZn[b]	5.0	phenylphosphate		0.0030 (0.0002)
GaZn[b]	5.0	phenylphosphate		0.14 (0.07)
FeZn[c]	5.5	*p*-NPP	5 (2)	0.43 (0.02)
FeZn[d]	6.0	*p*-NPP	3 (1)	0.79 (0.05)
FeZn[d]	6.5	*p*-NPP	3.4 (0.3)	2.05 (0.1)
FeFe[e]	6.5	*p*-NPP	4.8 (0.5)	4.44 (0.4)

[a] K_i values result from a fit of the entire data set at several fluoride concentrations to the Michaelis−Menten equation for mixed-competitive inhibition. Numbers in parentheses are standard deviation values obtained from the fitting procedure. [b] Assay conditions: 100 mM NaOAc, 200 mM KCl, pH 5.0, and 22 °C. [c] Assay conditions: 100 mM NaOAc, 200 mM KCl, pH 5.5, and 22 °C. [d] Assay conditions: 100 mM Na−MES, 200 mM KCl, and 22 °C. [e] Assay conditions: 100 mM Na-MES, 185 mM KCl, pH 6.5, and 22 °C; 15 mM Na-ascorbate, 0.2 mM $Fe(NH_4)_2(SO_4)_2$ and 22 °C.

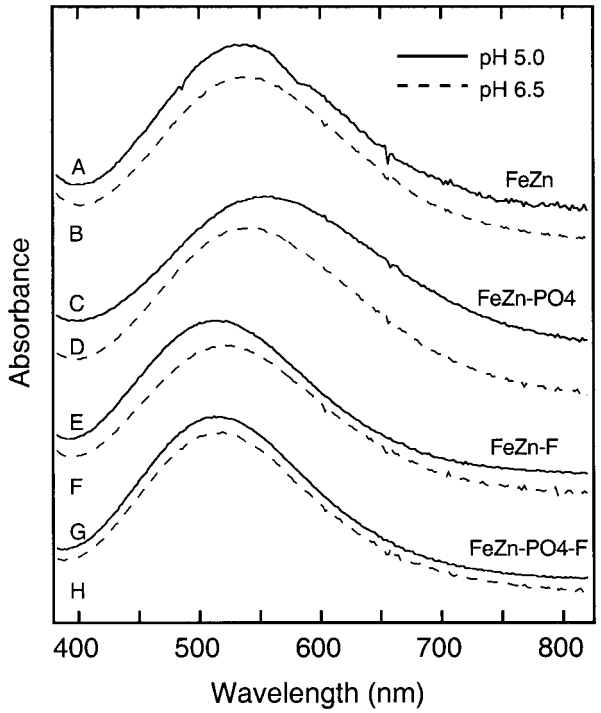

FIGURE 2: Effect of the addition of phosphate and/or fluoride on the visible spectra of FeZn−BSPAP at pH 5.0 and 6.5. Buffer: 100 mM NaOAc, 200 mM KCl, pH 5.0 or 100 mM Na-MES, 200 mM KCl, pH 6.5. (A) FeZn−BSPAP pH 5.0; (B) FeZn−BSPAP pH 6.5; (C) FeZn−BSPAP + 20 mM phosphate pH 5.0; (D) FeZn−BSPAP + 20 mM phosphate pH 6.5; (E) FeZn−BSPAP + 10 mM fluoride pH 5.0; (F) FeZn−BSPAP + 10 mM fluoride pH 6.5; (G) FeZn−BSPAP + 20 mM phosphate + 10 mM fluoride pH 5.0; (H) FeZn−BSPAP + 20 mM phosphate + 10 mM fluoride pH 6.5.

substrate. Figure 2 shows the effect of fluoride and/or phosphate on the position of the tyrosinate-to-Fe^{3+} charge-transfer band, both at pH 5 and pH 6.5. The uncomplexed enzyme has its maximal absorbance (λ_{max}) at ~536 nm, both at pH 5.0 and 6.5. As shown in the preceding paper, the spectra of FeZn−BSPAP·PO_4 are pH dependent, with a λ_{max} of 555 nm at pH 5.0 and a λ_{max} of 540 nm at pH 6.5. Fluoride binding to FeZn−BSPAP causes a blue shift of the absorption band, both at pH 5.0 and pH 6.5. The same blue shift is observed when fluoride is added to FeZn−BSPAP in the

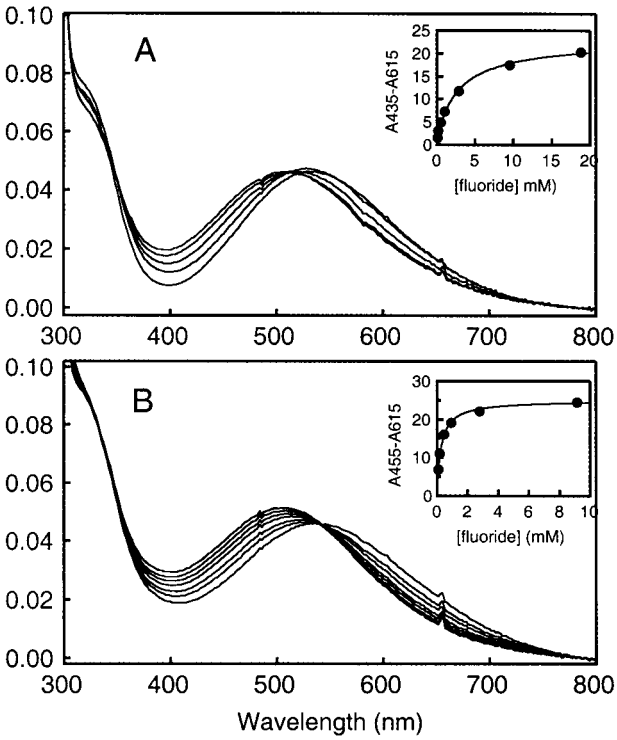

FIGURE 3: Optical titration of fluoride binding to (A) FeZn−BSPAP and (B) FeZn−BSPAP·PO_4 at pH 5.0. (A) FeZn−BSPAP in 100 mM NaOAc, 200 mM KCl, pH 5.0 with spectra taken at 0, 0.50, 3.0, 10, and 20 mM KF. (B) FeZn−BSPAP·PO_4 in 100 mM NaOAc, 200 mM KCl, 10 mM KH_2PO_4, pH 5.0 with spectra taken at 0, 0.10, 0.20, 0.50, 1.0, 3.0, and 10 mM KF. The arrows indicate increasing fluoride concentrations. The insets shows the absorbance difference as a function of fluoride concentration. The solid lines represent fits with K_d's of 2.9 and 0.28 mM, respectively.

presence of saturating concentrations of phosphate. The optical spectrum of this putative FeZn−BSPAP·PO_4·F complex is similar to that of FeZn−BSPAP·F, indicating that the ligand environment of the Fe^{3+} is similar in both complexes. Unlike the phosphate complexes, the FeZn−BSPAP·PO_4·F complexes are very similar at 5.0 and 6.5, suggesting that the same ternary complex is formed at both pHs.

Figure 3 shows fluoride titration experiments in the absence (A) and presence (B) of 10 mM phosphate at pH 5.0. The binding curves obtained by plotting the absorbance difference as a function of fluoride concentration yield a K_d of 2.9 ± 0.4 mM for fluoride binding to FeZn−BSPAP and a K_d of 0.28 ± 0.04 mM for fluoride binding to FeZn−BSPAP·PO_4. This latter K_d is in agreement with the inhibition constant of fluoride as determined by steady-state enzyme kinetics under similar conditions (K_i = 0.20 ± 0.03 mM).

Figures 4 and 5 show the EPR spectra of Fe(III)Zn(II)−BSPAP in the absence of any inhibitor and in the presence of phosphate and/or fluoride at pH 5.0 and 6.5, respectively. The EPR spectra of FeZn−BSPAP and FeZn−BSPAP·PO_4 have been reported before (*13*, *33*). The EPR spectrum of uncomplexed FeZn−BSPAP is the same at pH 5.0 and pH 6.5 and shows peaks that belong to several high-spin Fe^{3+} species with rhombicities of $E/D \sim 0.02$ (g = 6.5 and 5.9) and $E/D \sim 0.08$ (g = 7.7 and 5.8). At pH 5.0, the addition of phosphate converts this rather broad spectrum to an intense isotropic signal at g = 4.3, corresponding to the middle

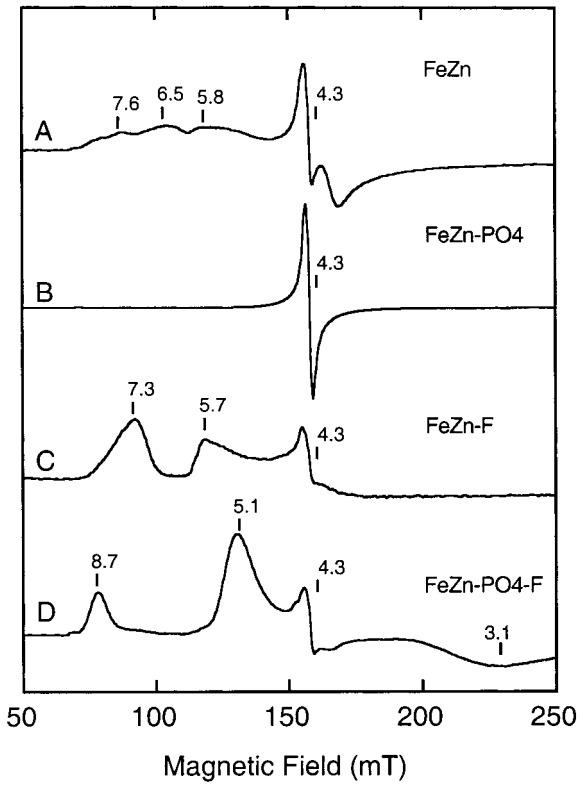

FIGURE 4: EPR spectra of (A) FeZn−BSPAP, (B) FeZn−BSPAP·PO_4, (C) FeZn−BSPAP·F, and (D) FeZn−BSPAP·PO_4·F in 100 mM NaOAc, 200 mM KCl, pH 5.0. The gains were adjusted to give similar signal heights. EPR conditions: microwave frequency, 9.4 GHz; modulation, 12.7 G at 100 kHz; microwave power, 2.0 mW; temperature, 10 K. FeZn−BSPAP·PO_4: 54 mM KH_2PO_4; FeZn−BSPAP·F: 3 mM KF; FeZn−BSPAP·PO_4·F: 49 mM KH_2PO_4 and 8.1 mM KF.

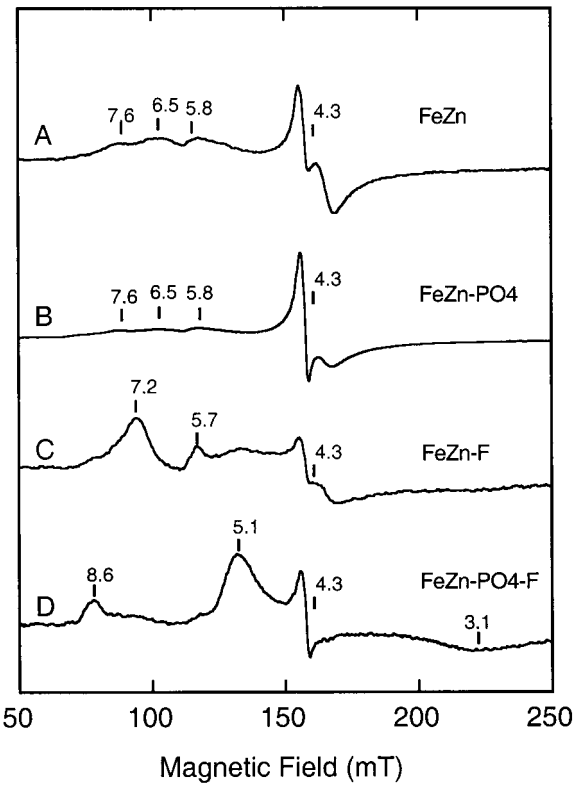

FIGURE 5: EPR spectra of (A) FeZn−BSPAP, (B) FeZn−BSPAP·PO_4, (C) FeZn−BSPAP·F, and (D) FeZn−BSPAP·PO_4·F in 100 mM Na−MES, 200 mM KCl, pH 6.5. The gains were adjusted to give similar signal heights. EPR conditions: microwave frequency, 9.4 GHz; modulation, 12.7 G at 100 kHz; microwave power, 8.0 mW; temperature, 10 K. FeZn−BSPAP·PO_4: 91 mM KH_2PO_4/K_2HPO_4; FeZn−BSPAP·F: 4 mM KF; FeZn−BSPAP·PO_4·F: 91 mM KH_2PO_4 and 4 mM KF.

Kramers doublet of a species with $E/D = 0.33$. At pH 6.5, addition of phosphate does not affect the EPR spectrum of FeZn−BSPAP significantly for [phosphate] < 30 mM, indicating that phosphate does not coordinate to the Fe^{3+} at this pH (*13*). The titration of FeZn−BSPAP with fluoride at pH 5.0 resulted in the formation of a species with peaks at $g = 7.3$ and 5.7 (Figure S3 of the Supporting Information). The $g = 7.3$ signal is ascribed to the ground doublet of a species with $E/D \approx 0.06$, and the $g = 5.7$ signal is probably due to the middle Kramers doublet of the same species. A fit of the difference of the signal intensities at $g = 7.3$ and 6.5 as a function of fluoride concentration yields a K_d of 0.13 mM. The EPR spectrum of the FeZn−BSPAP·F complex at pH 6.5 is similar to that at pH 5.0. The K_d for fluoride binding obtained from this EPR titration is 0.5 mM (Figure S4 of the Supporting Information).

When fluoride is added to FeZn−BSPAP·PO_4 yet another high-spin Fe^{3+} EPR-spectrum is obtained, and again the same spectrum is obtained both at pH 5.0 and pH 6.5. The EPR spectrum of this ternary FeZn−BSPAP·PO_4·F complex shows peaks at $g = 8.6$, 5.1, and 3.1. These features can again be ascribed to a single species with $E/D \approx 0.15$. The $g = 8.6$ signal belongs to the ground doublet, while the $g = 5.1$ and 3.1 signals are due to a transition in the middle Kramers doublet. The titration data yield K_d values of 0.06 mM and 0.9 mM at pH 5.0 and 6.5, respectively (Figures S5 and S6 of the Supporting Information). Like the optical spectra, the EPR spectra show that the same fluoride complexes are formed at pH 5.0 and 6.5. Moreover, the EPR spectrum of FeZn−BSPAP·PO_4·F is clearly different from those of FeZn−BSPAP·PO_4 and FeZn−BSPAP·F, providing direct spectroscopic evidence for the formation of a ternary complex. Fluoride addition (up to 15 mM) to the molybdate complex of FeZn−BSPAP at pH 5.0 does not result in any spectroscopic changes in either the optical or the EPR spectrum of FeZn−BSPAP·MoO_4.

In the course of the enzyme kinetics experiments, nonlinear product vs time curves were observed for AlZn−BSPAP in the presence of the (low) fluoride concentrations at which AlZn−BSPAP is inhibited. The initial rate decreased in time for approximately 1 min after mixing and then became constant. One explanation for this behavior is that fluoride binding is slow under these conditions, such that the formation of the fluoride complex is still not complete even after the 10 s required to mix the enzyme with substrate and inhibitor and place the cuvette in the spectrophotometer. Since our optical titration experiments showed that fluoride binds more strongly to FeZn−BSPAP in the presence of phosphate (and presumably also in the presence of substrate), this hypothesis cannot be tested by preincubation of the enzyme with fluoride. We probed whether biphasic progress curves could also be detected for FeZn−BSPAP using a hand stopped-flow apparatus that allowed mixing of enzyme with substrate and inhibitor within 0.5 s. Figure 6 shows reaction progress curves for the hydrolysis of *p*-NPP at pH 6.5 by FeZn−BSPAP in the absence and presence of various

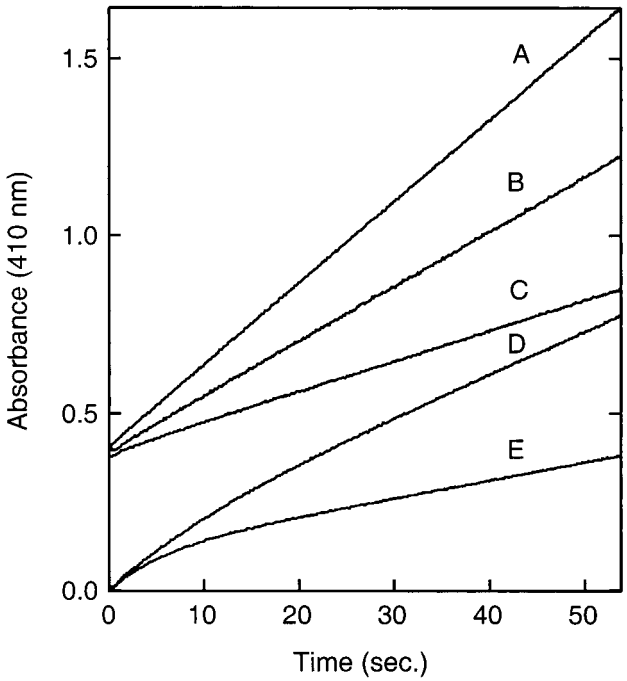

FIGURE 6: Reaction progress curves for the hydrolysis of *p*-NPP by FeZn−BSPAP after mixing with various inhibitors at pH 6.5 and 22 °C. At $t = 0$, FeZn−BSPAP was rapidly mixed with 50 mM *p*-NPP and (A) no inhibitor, (B) 1.0 mM phosphate, (C) 100 μM molybdate, (D) 2.0 mM KF, and (E) 8.0 mM KF. Buffer: 100 mM Na-MES, 200 mM KCl, pH 6.5.

inhibitors. Biphasic progress curves are observed only in the presence of fluoride but not in the presence of the oxoanion inhibitors phosphate and molybdate. Thus, the effect is specific for fluoride.

To prove that the nonlinear progress curves are indeed due to slow binding of fluoride to the enzyme−substrate complex, the formation of the ternary FeZn−BSPAP·PO_4·F complex was studied using time-resolved optical and EPR spectroscopy at pH 5.0. FeZn−BSPAP was rapidly mixed with 25 mM phosphate and 1 mM fluoride using a hand stopped-flow apparatus, and optical spectra were taken every second using a diode-array spectrophotometer. Figure 7A shows difference spectra obtained by subtracting the spectrum of FeZn−BSPAP·PO_4·F at equilibrium from the spectra obtained at various time points after mixing. The spectra show a clear blue-shift of the absorbance with time, consistent with conversion of FeZn−BSPAP·PO_4 to FeZn−BSPAP·PO_4·F. The absorbance at 620 nm could be fitted by a single exponential with a rate constant of 0.173 ± 0.003 s^{-1}. This rate is in reasonable agreement with the value of k_{obs} obtained from the reaction progress curves obtained under similar conditions (FeZn−BSPAP, 25 mM phenyl phosphate, and 1 mM fluoride), which is 0.14 ± 0.02 s^{-1}. The time dependence of the formation of FeZn−BSPAP·PO_4·F was also studied by EPR spectroscopy. FeZn−BSPAP was rapidly mixed with 1 mM fluoride and 25 mM phosphate and injected into EPR tubes. At various times after mixing, the samples were rapidly frozen in a bath of cold isopentane (~140 K). Figure 7B shows the conversion of FeZn−BSPAP·PO_4 ($g = 4.3$) into FeZn−BSPAP·PO_4·F ($g = 8.6$ and 5.1). Fits of the intensities at $g = 4.3$ and $g = 5.1$ as a function of time gave rate constants of 0.158 ± 0.004 s^{-1} and 0.13 ± 0.05 s^{-1}, respectively, again in good agreement with the rate constants that were obtained from the reaction progress curve and the time dependent optical changes discussed above.

Together, these results firmly establish that the biphasic reaction progress curves are due to the slow binding of fluoride to the enzyme−substrate complex. If it is assumed that inhibitor binding is much slower than substrate binding and substrate hydrolysis (in the absence of fluoride, the steady state is reached within a few ms), the time dependence

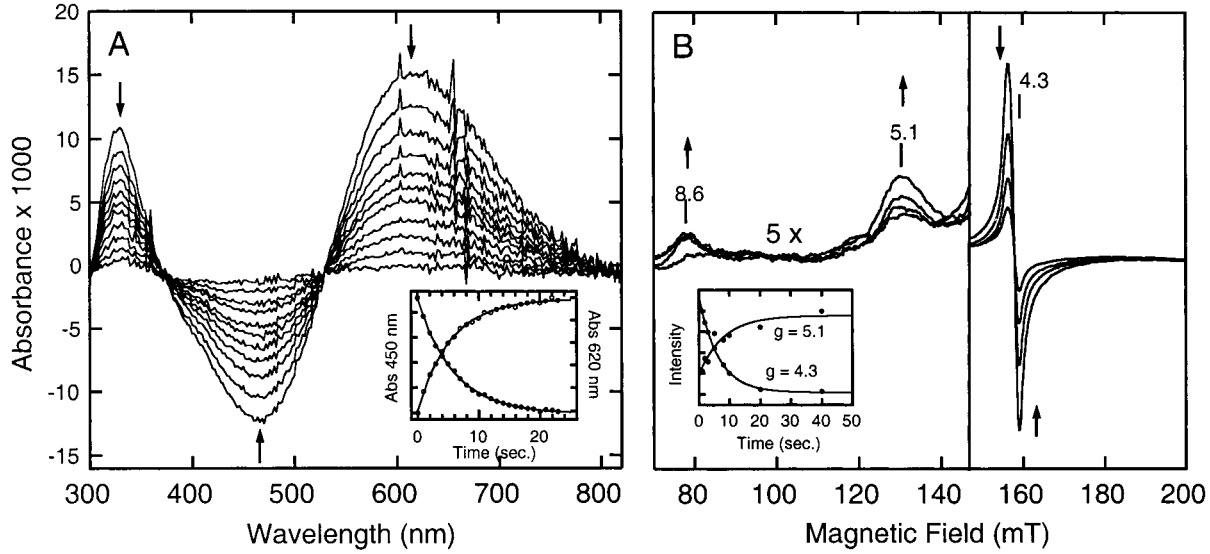

FIGURE 7: Time-resolved spectroscopy of the formation of FeZn−BSPAP·PO_4·F at pH 5.0 and 22 °C. (A): FeZn−BSPAP was rapidly mixed with 25 mM KH_2PO_4 and 1 mM KF. Shown are difference spectra obtained by subtraction of the optical spectrum of FeZn−BSPAP·PO_4·F at t > 60 s. from the optical spectra at $t = 1$, 2, 3, 4, 5, 6, 7, 9, 11, 15, and 24 s. Buffer: 100 mM NaOAc, 200 mM KCl, pH 5.0. Inset: absorbance at 450 and 620 nm as a function of time. The solid lines represent single-exponential fits with rate constants of 0.195 ± 0.006 s^{-1} (A_{450}) and 0.173 ± 0.003 s^{-1} (A_{620}). (B) EPR spectra of FeZn−BSPAP that was rapidly mixed with 25 mM KH_2PO_4 and 1 mM KF, and freeze-quenched after 1, 5, 20 and 40 s. Buffer: 100 mM NaOAc, 200 mM KCl, pH 5.0. EPR conditions: microwave frequency, 9.42 GHz; modulation, 12.7 G at 100 kHz; microwave power, 8.0 mW; temperature, 10 K. Inset: intensities of the $g = 4.3$ and $g = 5.1$ signals as a function of time. The solid lines represent single-exponential fits with rate constants of 0.158 ± 0.004 s^{-1} ($g = 4.3$) and 0.125 ± 0.05 s^{-1} ($g = 5.1$).

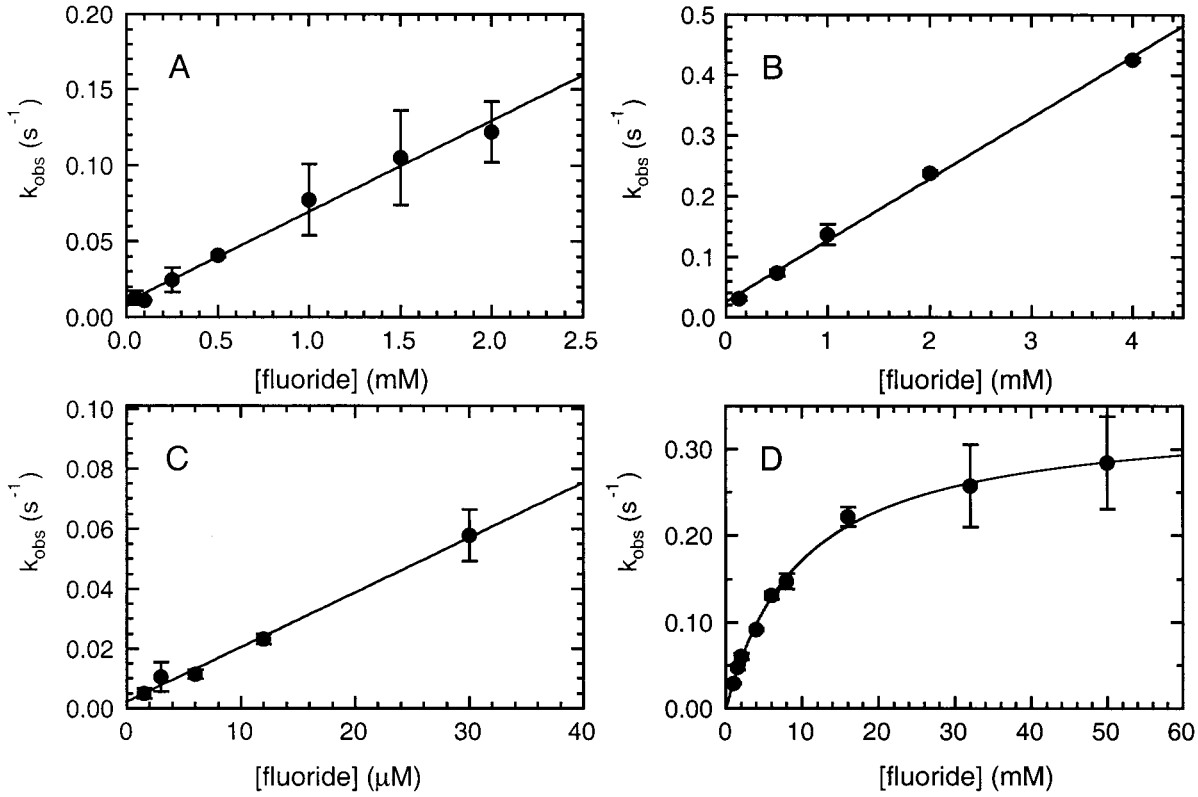

FIGURE 8: Rate of fluoride binding (k_{obs}) as a function of fluoride concentration for (A) FeFe−BSPAP at pH 5.0, (B) FeZn−BSPAP at pH 5.0, (C) AlZn−BSPAP at pH 5.0, and (D) FeZn−BSPAP at pH 6.5. Each data point represents the average of ≥ 3 measurements; the error bars indicate the standard deviation. Conditions: pH 6.5: 100 mM Na-MES, 200 mM KCl, 50 mM *p*-NPP at 22 °C; pH 5.0: 100 mM Na-MES, 200 mM KCl, 25 mM phenyl phosphate at 22 °C.

of product concentration is described by the general eq 2 (*34*, *35*).

$$P_{(t)} = v_i t + (v_i - v_{ss})(1 - e^{(-k_{obs}t)})/k_{obs} + P_{(0)}$$

(v_i: initial rate at $t = 0$, v_{ss}: rate in final steady-state) (2)

Thus, the rate of fluoride binding (k_{obs}) can be obtained by fitting the product formation traces using eq 2. Enzyme was rapidly mixed with substrate and fluoride using a hand-stopped flow and the formation of phenol (pH 5.0) or *p*-nitrophenol (pH 6.5) was monitored spectrophotometrically. The rate of fluoride binding was determined as a function of fluoride concentration for FeZn−BSPAP at pH 5.0 and 6.5 (Figure 8, B and D). The influence of the chemical nature of the metals was studied by measuring k_{obs} values as a function of fluoride concentration for FeFe−BSPAP and AlZn−BSPAP at pH 5.0 (Figure 8, A and C). Fluoride binding for other combinations were not studied because fluoride binding was either too fast (GaZn−BSPAP) or too slow (AlZn−BSPAP at pH 6.5) or because the enzyme was not stable enough in the absence of fluoride during the time course of the reaction (FeFe−BSPAP at pH 6.5).

Figure 8 shows that at pH 5.0 k_{obs} depends linearly on the fluoride concentration for all BSPAP forms. At this pH, fluoride inhibition is uncompetitive. Since [S] ≫ K_M, the process that is studied under these conditions is the binding of fluoride to the enzyme−substrate complex at the uncompetitive fluoride binding site (Scheme 2). For this mechanism, the observed rate constant, k_{obs}, is related to the fluoride

Scheme 2

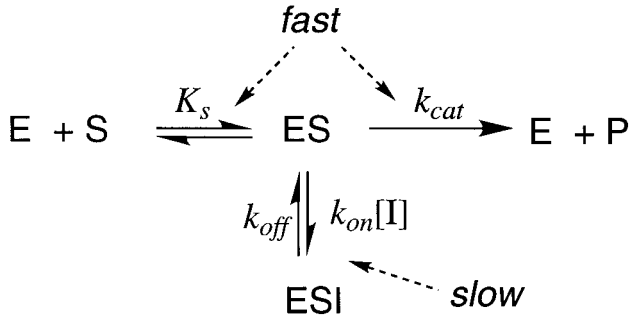

concentration and the intrinsic rate constants k_{on} and k_{off} by eq 3.

$$k_{obs} = k_{on}[I] + k_{off} \quad (3)$$

Table 2 lists values for k_{on} and k_{off} for FeZn−, AlZn−, and FeFe−BSPAP at pH 5.0. Because fluoride release is so slow, our data do not allow an accurate determination of k_{off}; Table 2, therefore, lists upper limits.

At pH 6.5, the k_{obs} value for fluoride binding to FeZn−BSPAP is no longer linearly dependent on the fluoride concentration, but instead saturating behavior is observed. This kinetics behavior indicates that a preequilibrium is formed rapidly (formation of ESI′), followed by the slower formation of the catalytically inactive inhibitor complex ESI″ (Scheme 3). Equation 4 describes the dependence of k_{obs} on k_{on}, k_{off} and the dissociation constant K_d for this mechanistic scheme. In principle, fluoride binding at pH 6.5 may involve binding to both the competitive site and the uncompetitive

Table 2: Rate Constants for Fluoride Binding[a]

enzyme	pH	k_{on}	k_{off} (s^{-1})
FeZn[b]	6.5	0.33 (0.01) s^{-1}	<0.02
FeZn[c]	5.0	$102 \pm 3\ s^{-1}\cdot M^{-1}$	<0.03
AlZn[c]	5.0	$1.8 \pm 0.2 \cdot 10^3\ s^{-1}\cdot M^{-1}$	<0.003
FeFe[c]	5.0	$58 \pm 5\ s^{-1}\cdot M^{-1}$	<0.02

[a] Rate constants for fluoride binding were derived by fitting the k_{obs} vs fluoride concentration plots in Figure 8. [b] Values of k_{on} and k_{off} result from a fit using eq 4 (K_d = 10 mM). [c] Values of k_{on} and k_{off} result from a fit using eq 3.

Scheme 3

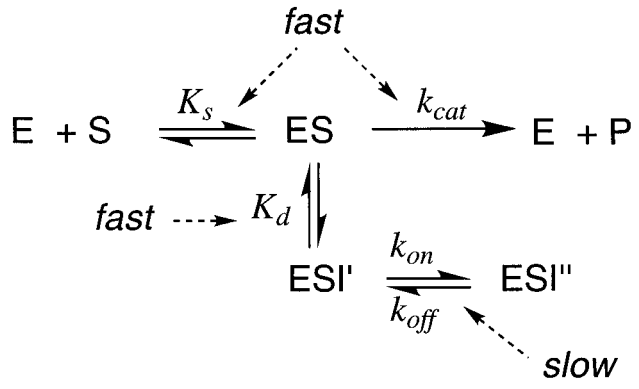

site. Binding at the competitive site is unlikely to contribute directly to the slow inhibition phenomenon, however, since fluoride binding to the divalent metal ion is expected to be much faster than fluoride binding to the uncompetitive site (Fe^{3+}). The data in Figure 8D could be fitted with K_d = 10 mM, k_{on} = 0.33 s^{-1}, and $k_{off} \leq 0.02\ s^{-1}$ (Table 2).

$$k_{obs} = k_{on}[I]/([I] + K_d) + k_{off} \quad (4)$$

DISCUSSION

Fluoride is a well-known inhibitor of metalloenzymes, such as peroxidase (*36*), laccase (*37*), inorganic pyrophosphatase (*38*−*40*), *myo*-inositol monophosphatase (*41*), enolase (*42*), superoxide dismutase (*43*), urease (*44*), and various zinc-containing hydrolases (*29*, *45*, *46*). Fluoride inhibition has been reported for various PAPs, including BSPAP. Non-competitive (*21*, *22*, *25*, *47*) and uncompetitive inhibition (*17*, *24*) modes have been reported for PAPs, with inhibition constants of typically ~1 mM. Our results show that the inhibition mode of fluoride is pH dependent, which may explain why previous studies have reported both noncompetitive and uncompetitive inhibition by fluoride. A similar pH dependence for the fluoride inhibition mode has been reported for the native PAP isolated from sweet potatoes (*24*). We do not observe the curvilinear Lineweaver−Burke plots that were reported previously for (native) BSPAP (*15*, *16*), possibly as a result of the higher ionic strength employed by us.

In most metalloenzymes, fluoride is thought to act by replacing a metal-bound hydroxide or water ligand. The X-ray structure of KBPAP shows three coordination sites at the dimetal center that have been proposed to contain water-derived ligands: a hydroxide bridging the two metals, a hydroxide acting as a monodentate ligand to Fe^{3+}, and a water coordinating to Zn^{2+} (*4*). In the preceding paper, we suggested that substrate binds in a monodentate fashion to the divalent metal ion in the catalytically active enzyme−substrate complex formed at pH 6.5. Fluoride binding to the divalent metal ion is then likely to be responsible for the competitive inhibition mode. For the uncompetitive binding mode, two possibilities may be considered: fluoride replacing the monodentate hydroxide/water bound to the Fe^{3+} or the μ-hydroxo group that is bound to both the Fe^{3+} and the divalent metal ion. The strong binding observed for Al^{3+} in AlZn−BSPAP is in agreement with the Hard−Soft-Acid−Base theory: fluoride is a hard base and Al^{3+} is a harder acid than both Fe^{3+} and Ga^{3+}. The relative binding strength of fluoride vs water is, therefore, expected to be higher for Al^{3+} than for either Fe^{3+} or Ga^{3+}. The much stronger inhibition of AlZn−BSPAP compared to FeZn−BSPAP and GaZn−BSPAP indicates that the uncompetitive fluoride binding site is at the trivalent metal ion, but does not distinguish between a terminal or bridging binding mode. The pH dependence of $K_{i(uncomp)}$ parallels the pK_a of the Fe^{3+} coordinated water in the enzyme−substrate complex, suggesting that fluoride binds by replacing this terminal water/hydroxide. This model predicts that the ternary enzyme−substrate/fluoride complex that is formed is the same at pH 6.5 and 5.0 (Figure 9). At pH 6.5, fluoride binds to the enzyme−substrate complex by replacing the terminal hydroxide ligand to Fe^{3+}, yielding a ternary complex with substrate bound at the divalent metal and fluoride bound at the trivalent metal. At pH 5.0, fluoride binds to the enzyme−substrate-complex by displacing the substrate from the trivalent metal, yielding again a ternary complex with substrate bound at the divalent metal and fluoride bound at the trivalent metal.

The model derived from the kinetics results was tested by studying the optical and EPR spectroscopic properties of FeZn−BSPAP·F and FeZn−BSPAP·PO_4·F complexes at pH 6.5 and 5.0. FeZn−BSPAP, FeZn−BSPAP·PO_4, FeZn−BSPAP·F, and FeZn−BSPAP·PO_4·F each have their own characteristic EPR spectrum, providing direct spectroscopic evidence for the formation of a ternary FeZn−BSPAP·PO_4·F complex. The optical spectra of FeZn−BSPAP·F and FeZn−BSPAP·PO_4·F are practically indistinguishable, indicating a similar electron density at Fe^{3+} in these two complexes. The blue-shift of the tyrosinate to Fe^{3+} charge-transfer band has been reported in previous studies on fluoride binding to PAP (*15*, *16*) and suggests an increase in electron density at Fe^{3+} upon fluoride binding. The EPR and optical spectra of FeZn−BSPAP·F and FeZn−BSPAP·PO_4·F are pH independent and are, therefore, consistent with the model derived from enzyme kinetics (Figure 9). Although the model depicted in Figure 9 provides the simplest explanation for our results, other fluoride binding modes (i.e., fluoride replacing the bridging hydroxide) cannot be excluded. More direct information on the structure of the ternary enzyme−phosphate−fluoride complex must await future characterization of these complexes using X-ray diffraction, EXAFS, or possibly ENDOR/ESEEM.

The K_d for fluoride binding to FeZn−BSPAP·PO_4 obtained from the optical titration at pH 5.0 (0.28 ± 0.04 mM) compares nicely with the inhibition constant for fluoride obtained under similar condions (0.20 ± 0.03 mM). The large difference in fluoride affinity between FeZn−BSPAP (K_d = 2.9 mM) and FeZn−BSPAP·PO_4 (K_d = 0.20 ± 0.03 mM) suggests that fluoride needs to replace a hydroxide when

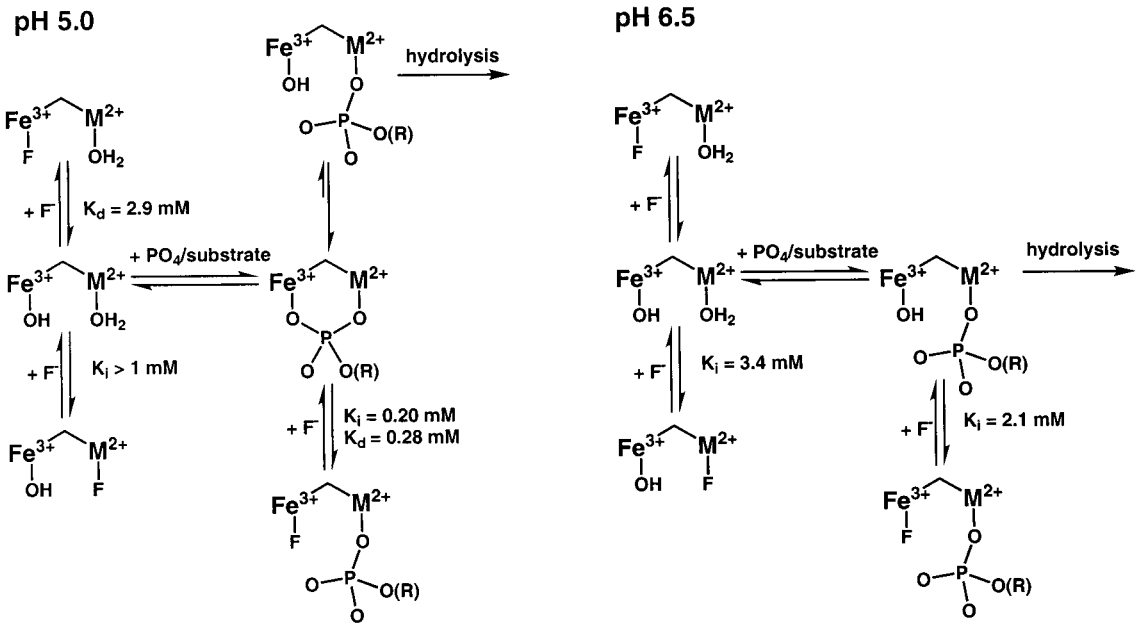

FIGURE 9: Model for the coordination of fluoride, phosphate, and phosphate ester to FeZn−BSPAP at both pH 5.0 and pH 6.5. The model explains the results of both the kinetics and spectroscopic experiments described in this work.

binding to FeZn−BSPAP, while it needs to replace the less strongly bound bridging phosphate in FeZn−BSPAP·PO_4. The K_d values obtained from the various EPR titrations are all lower than those obtained from the optical titration and kinetics experiments. The largest discrepancy in the dissociation constant is observed between the optical and EPR titration of fluoride binding to FeZn−BSPAP at pH 5.0 (K_d = 2.9 mM and K_d = 0.13 mM, respectively). Because neither the optical titration nor the EPR titration gives any indication for two binding events (e.g., no EPR spectral changes are detected between 1 and 3 mM fluoride, while no major changes are detected in the optical spectra between 0 and 0.5 mM), we think that the UV−vis changes and the changes detected by EPR correspond to the same process. The lower dissociation constants determined by EPR may be due to the lower temperature (freezing point of the solution) at which they were determined.

Unlike phosphate, molybdate cannot be displaced from the Fe^{3+} site by fluoride, which corroborates conclusions from previous studies that divided the oxoanions into two classes, the weak inhibitors phosphate and arsenate and the strong inhibitors molybdate and tungstate (*10*, *16*, *28*, *48*). On the basis of EXAFS studies of oxoanion complexes with FeZn−Uf at pH 5.0, Wang and Que recently proposed an unsymmetric bridging coordination for molybdate and tungstate with strong binding to the Fe^{3+} and weak binding to the Zn^{2+} (*11*, *12*). This strong binding to the Fe^{3+} may explain why fluoride is not able to displace molybdate from this site, while it does displace phosphate or substrate.

A surprising result from these studies is that fluoride, unlike the oxoanions phosphate and molybdate, is a slow-binding inhibitor of BSPAP. Substitution reactions at hexacoordinated Fe^{3+} are generally dissociative in nature. This means that the on rate for fluoride binding may be limited by the rate of dissociation of the ligand that is replaced by fluoride, while the off rates are limited by the dissociation rate for fluoride. The spectroscopic results of this study and of the structure of the phosphate complex described in the preceding paper suggest that fluoride binding to the enzyme−substrate complex at pH 5.0 involves displacement of the substrate at the trivalent metal ion. The on rates of fluoride binding at pH 5.0 may, therefore, reflect the intrinsic rate at which phenyl phosphate dissociates from this trivalent metal ion. For FeZn−BSPAP and FeFe−BSPAP, these rates are 100 and 60 M^{-1} s^{-1}, respectively, while for AlZn−BSPAP the rate is 1800 M^{-1} s^{-1}. Since we cannot exclude the formation of a preequilibrium with a K_d > 10 mM (or K_d > 0.1 mM for AlZn), the true dissociation rates may be lower, and these numbers should be regarded as upper limits. Although we can only determine upper limits for k_{off}, it is clear that the rate of fluoride dissociation from either Fe^{3+} or Al^{3+} in M(III)Zn(II)−BSPAP is very slow (<0.03 and < 0.003 s^{-1}, respectively (Table 2)). Future studies using methods suited to determine these low off rates may give more accurate values of k_{off} and allow the aluminum and iron enzymes to be compared.

The hyperbolic dependence of k_{obs} on fluoride concentration at pH 6.5 indicates the formation of an enzyme-fluoride complex prior to the formation of the inhibited fluoride form. The nature of this species is unknown. One possibility is that the fluoride binds initially at the divalent metal ion (the competitive binding site). The value of the apparent K_d is roughly consistent with this interpretation.[2] The value of k_{on} obtained from this experiment is a true first-order rate constant and is very low, only 0.33 s^{-1}. This low rate is consistent with our model for the phosphate/substrate complex at pH 6.5, which predicts that fluoride binds to the Fe^{3+} by replacing a hydroxide. Dissociation of the hydroxide is expected to be slower than the release of the substrate that needs to take place at pH 5.0.

Slow binding of fluoride has been observed for other metalloenzymes as well. Baykov et al. studied the slow

[2] Since fluoride and substrate compete for the same binding site in this model, the apparent dissociation constant for fluoride binding to this site is: $K_d = K_i \times ([S]+K_M)/K_M$ = 3.4 mM × (50 mM + 10 mM)/10 mM = 20.4 mM.

binding of fluoride to pyrophosphatases and interpreted their results in a model that involved the formation of a quaternary enzyme−Mg−PP_i−F complex (*38*−*40*). Fluoride binding to urease, an enzyme that also possesses a dinuclear metal site containing two Ni ions, is even more relevant to the present study (*44*). In urease, fluoride binds rapidly to a competitive site with a K_d of 1 mM, but fluoride binding to an uncompetitive site was shown to be slow and to have a K_d of 0.2 mM. The rates of slow fluoride binding observed by these authors were 0.008−0.038 s^{-1}, which are in the same range as the rates observed in this work. Slow inhibitor binding is normally associated with very tight binding inhibitors, with binding constants <1 nM (*34*), but fluoride binding to PAP and the enzymes mentioned above is rather weak (μM to mM range). Molybdate and fluoride both bind to the PAP active site and both do so by displacing the same ligands, so why is slow binding only observed for fluoride and not for molybdate? Binding of the oxoanions involves the fast formation of a preequilibrium in which the oxoanion binds at the divalent metal ion, followed by slower coordination to Fe^{3+} (*49*−*51*). Most of the stablility of the oxoanion complexes is derived from interactions with amino acid side chain residues, such as histidines. For fluoride, which has fewer possible interaction modes with these amino acids, the binding strength may be due almost exclusively to its interaction with the metal ion, and no preequilibrium should exist. This in turn means that at inhibitor concentrations around K_d ([I] = K_d), k_{on}[I] ≈ k_{off}, and, therefore, k_{obs} ≈ 0.5·k_{off}. For an inhibitor with the same values of k_{on}, k_{off} and overall K_d, but now with a preequilibrium such that e.g. $K_{d(preequil)}$ = 5 × K_d, k_{on}[I]/([I] + $K_{d(preequil)}$) = k_{on}/6 and, therefore, k_{obs} ≈ k_{on}/6 and ≫ k_{off}. The slow binding of fluoride often observed for metalloenzymes may thus result from the fact that its rate is determined by the slow dissociation rate of fluoride from a metal ion and the absence of other interactions besides metal coordination that contribute to its stablility.

ACKNOWLEDGMENT

We thank Winfried Roseboom for his helpful suggestions on the rapid-mixing rapid-freezing experiment. This research was supported in part by the EC Biotechnology Program.

SUPPORTING INFORMATION AVAILABLE

Lineweaver−Burke plots of inhibition of various BSPAP forms by fluoride (Figure S1), replots of $1/K_{M(app)}$ and $1/V_{max(app)}$ as a function of fluoride concentration for various BSPAP forms (Figure S2), and EPR fluoride titration experiments for FeZn−BSPAP and FeZn−BSPAP·PO_4 at pH 5.0 and 6.5 (Figures S3−S6). This material is available free of charge via the Internet at http://pubs.acs.org.

REFERENCES

1. Sträter, N., and Lipscomb, W. N. (1995) *Biochemistry 34*, 14792−14800.
2. Wilcox, D. E. (1996) *Chem. Rev. 96*, 2435−2458.
3. Klabunde, T., and Krebs, B. (1997) *Structure and Bonding 89*, 177−198.
4. Sträter, N., Klabunde, T., Tucker, P., Witzel, H., and Krebs, B. (1995) *Science 268*, 1489−1492.
5. Klabunde, T., Sträter, N., Fröhlich, R., Witzel, H., and Krebs, B. (1996) *J. Mol. Biol. 259*, 737−748.
6. Klabunde, T., Sträter, N., Krebs, B., and Witzel, H. (1995) *FEBS Lett. 367*, 56−60.
7. Koonin, E. V. (1994) *Protein Sci. 3*, 356−368.
8. Zhuo, S., Clemens, J. C., Stones, R. L., and Dixon, J. E. (1994) *J. Biol. Chem. 269*, 26234−26238.
9. Merkx, M., and Averill, B. A. (1999) *J. Am. Chem. Soc.*, in press.
10. David, S. S., and Que, L., Jr. (1990) *J. Am. Chem. Soc. 112*, 6455−6463.
11. Wang, X., Randall, C. R., True, A. E., and Que, L., Jr. (1996) *Biochemistry 35*, 13946−13954.
12. Wang, X., and Que, L., Jr. (1998) *Biochemistry 37*, 7813−7821.
13. Merkx, M., Pinkse, W. H., and Averill, B. A. (1999) *Biochemistry 38*, 9914−9925.
14. Mueller, E. G., Crowder, M. W., Averill, B. A., and Knowles, J. R. (1993) *J. Am. Chem. Soc. 115*, 2974−2975.
15. Davis, J. C., Lin, S. S., and Averill, B. A. (1981) *Biochemistry 20*, 4062−4067.
16. Vincent, J. B., Crowder, M. W., and Averill, B. A. (1991) *Biochemistry 30*, 3025−3034.
17. Robinson, D. B., and Glew, R. H. (1980) *J. Biol. Chem. 255*, 5864−5870.
18. Anderson, T. R., and Toverud, S. U. (1986) *Arch. Biochem. Biophys. 247*, 131−139.
19. Anderson, G., Ek-rylander, B., and Hammerström, L. (1984) *Arch. Biochem. Biophys. 228*, 431−38.
20. Schlosnagle, D. C., Sander, E. G., Bazer, F. W., and Roberts, R. M. (1976) *J. Biol. Chem. 251*, 4680−4685.
21. Rezyapkin, V. I., Leonova, L. E., and Komkova, A. I. (1985) *Biokhimiya 50*, 1067−1075.
22. Hayman, A. R., Warburton, M. J., Pringle, J. A. S., Coles, B., and Chambers, T. J. (1989) *Biochem. J. 261*, 601−609.
23. Antanaitis, B. C., and Aisen, P. (1985) *J. Biol. Chem. 260*, 751−756.
24. Kawabe, H., Sugiura, Y., Terauchi, M., and Tanaka, H. (1984) *Biochim. Biophys. Acta 784*, 81−89.
25. Hara, A., Sawada, H., Kato, T., Nakayama, T., Yamamoto, H., and Matsumoto, Y. (1984) *J. Biochem. 95*, 67−74.
26. Crowder, M. W., Vincent, J. B., and Averill, B. A. (1992) *Biochemistry 31*, 9603−9608.
27. Lau, K.-H. W., and Baylink, D. J. (1998) *J. Bone Min. Res 13*, 1660−1664.
28. Dietrich, M., Münstermann, D., Suerbaum, H., and Witzel, H. (1991) *Eur. J. Biochem. 199*, 105−113.
29. Chen, G. J., Edwards, T., Dsouza, V. M., and Holz, R. C. (1997) *Biochemistry 36*, 4278−4286.
30. Merkx, M., and Averill, B. A. (1998) *Biochemistry 37*, 8490−8497.
31. de Vries, S., Albracht, S. P. J., Berden, J. A., and Slater, E. C. (1982) *Biochim. Biophys. Acta 681*, 41−53.
32. Segel, I. H., *Enzyme Kinetics: Behaviour and analysis of rapid equilibrium and steady-state enzyme systems*. 1993, New York: John Wiley & Sons.
33. Merkx, M., and Averill, B. A. (1998) *Biochemistry 37*, 11223−11231.
34. Cha, S. (1975) *Biochem. Pharmac. 24*, 2177−2185.
35. Cha, S. (1976) *Biochem. Pharmac. 25*, 1561.
36. Neri, F., Kok, D., Miller, M. A., and Smulevich, G. (1997) *Biochemistry 36*, 8947−8953.
37. Bränden, R., Malmström, B. G., and Vänngård (1973) *Eur. J. Biochem. 36*, 195−200.
38. Baykov, A. A., Artjukov, A. A., and Avaeva, S. M. (1976) *Biochim. Biophys. Acta 429*, 982−992.
39. Baykov, A. A., Bakuleva, N. P., Nazarova, T. I., and Avaeva, S. M. (1977) *Biochim. Biophys. Acta 481*, 184−194.
40. Baykov, A. A., Alexandrov, A. P., and Smirnova, I. N. (1992) *Arch. Biochem. Biophys. 294*, 238−243.
41. Ganzhorn, A. J., and Chanal, M.-C. (1990) *Biochemistry 29*, 6065−6071.
42. Maurer, P. J. (1981) *Biochemistry 20*, 6894−6900.

43. Meier, B., Scherk, C., Schmidt, M., and Parak, F. (1998) *Biochem. J. 331*, 403−407.
44. Dixon, N. E., Blakeley, R. L., and Zerner, B. (1980) *Can. J. Biochem. 58*, 481−488.
45. Matthews, B. W. (1988) *Acc. Chem. Res. 21*, 333−340.
46. Christianson, D. W., and Lipscomb, W. N. (1989) *Acc. Chem. Res. 22*, 62−69.
47. Kato, T., Hora, A., Nakayama, T., Sawada, H., Hamatake, M., and Matsumoto, Y. (1986) *Comp. Biochem. Physiol. B 83*, 813−817.
48. Wang, D. L., Holz, R. C., David, S. S., Que, L., Jr., and Stankovich, M. T. (1991) *Biochemistry 30*, 8187−8194.
49. Aquino, M. A. S., Lim, J.-S., and Sykes, A. G. (1994) *J. Chem. Soc., Dalton Trans.* 429−436.
50. Aquino, M. A. S., Lim, J.-S., and Sykes, A. G. (1992) *J. Chem. Soc., Dalton Trans.* 2135−2136.
51. Lim, J.-L., Aquino, M. A. S., and Sykes, A. G. (1996) *Inorg. Chem. 35*, 614−618.

BI990446W